

Specific effect of hydrogen implantation in yttrium iron garnet and annealing behavior studied by conversion-electron Mössbauer spectroscopy

G. Marest

Institut de Physique Nucléaire (et Institut National de Physique Nucléaire et de Physique des Particules), Université Claude Bernard (Lyon 1), 43 boulevard du 11 Novembre 1918, 69622 Villeurbanne Cédex, France

A. Perez

Département de Physique des Matériaux, Université Claude Bernard (Lyon 1), 43 boulevard du 11 Novembre 1918, 69622 Villeurbanne Cédex, France

P. Gerard

Laboratoire d'Electronique et de Technologie de l'Informatique (LETI), Institut de Recherche Technologique et de Développement Industriel, Commissariat à l'Energie Atomique, Centre d'Etudes Nucléaires de Grenoble, Boite Postale 85X, 38041 Grenoble, France

J. M. Mackowski

Institut de Physique Nucléaire (et Institut National de Physique Nucléaire et de Physique des Particules), Université Claude Bernard (Lyon 1), 43 boulevard du 11 Novembre 1918, 69622 Villeurbanne Cédex, France

(Received 22 July 1985)

Conversion-electron Mössbauer-spectroscopy technique applied to ^{57}Fe -enriched yttrium iron garnet has allowed us to obtain good resolution of the spectra characteristic of the different iron sites. Its association with infrared spectroscopy has permitted us to show clearly the specific chemical effect of hydrogen implantation in comparison with a pure damage effect from a shallow neon implantation. Ne and H implantations affect preferentially the tetrahedral sites by changing the magnitude and directions of magnetizations. Moreover, for H implantation the presence of a new " d_{H} " magnetic site among the tetrahedral sites has been clearly correlated with the formation of O-H bonds. However, this effect concerns only about 15% of the implanted hydrogen; the remaining part responsible for the reduction of iron gives rise to the observation of characteristic effects on the Mössbauer spectra (line broadenings, hyperfine-field decreases, etc.). From the thermal-annealing behavior of H-implanted crystals two stages can be distinguished: Up to 350°C, when hydrogen is still present in the implanted volume, different evolutions of the Mössbauer spectra compared to those of a Ne-implanted crystal are observed; above 350°C, when hydrogen is completely diffused out of the garnet, the evolutions are similar except for the magnetization directions of d' sites and the persistence of the d_{H} component up to 850°C.

I. INTRODUCTION

Magnetic single-crystal films of garnets have been mainly used to make bubble memories¹ and to a lesser extent in magneto-optical displays and devices.^{2,3} The basic material is made from substitution in $\text{Y}_3\text{Fe}_5\text{O}_{12}$ (YIG). Above all, ion implantation has been applied as part of the elaboration of bubble memories. Most of the work in this field has sought a correlation between the depth profile of the ion implant, the concentration, and the nature of the structural disorder, the magnetic properties and the evolution of these parameters after subsequent annealing treatments.⁴ The outcome is the study of the macroscopic physical properties such as mechanical or magnetic characteristics.

The other trend is to look for the microscopic influence of damage and implants on the different matrix elements of the garnet. It can be done by conversion-electron

Mössbauer spectroscopy (CEMS) which yields direct information on iron interactions at site level. Moreover, this is a suitable technique to probe depths of about 100 nm compatible with the study of implanted layers.

Many contributions using the first approach are devoted to the comparison of implanted garnets with H^+ and Ne^+ in order to understand the peculiar action of hydrogen on the magnetic properties of garnets.⁴⁻⁹ Others are concerned with the microscopic approach by CEMS, first on neon¹⁰⁻¹³ and more recently on hydrogen^{14,15} implantations. In this case it was shown that in order to obtain a suitable fit a new site had to be taken into account for the H^+ - as compared to the Ne^+ -implanted bubble garnet. On the whole, hydrogen having a smaller mass than neon requires much higher doses to reach the same proper strain. It follows that (i) the amount of hydrogen in the garnet is sufficient to interact chemically or to exert internal pressures due to its sole presence within the material⁹ and (ii) the ion scattering process as calculated by Matsu-

tera *et al.*¹⁶ indicates that most of the damage produced by H implantation is caused by small oxygen-nuclei displacements, whereas Ne severely injures the garnet lattice.

The aim of the present study is to compare the H- and Ne-implantation effects in YIG using CEMS. In absorption measurements have been made to complement the Mössbauer results. Pure YIG was chosen on account of the fact that it is the prototype for bubble garnet materials and, above all, that without any diamagnetic substitution, the Mössbauer linewidths are thin, allowing fine-detail observations. In the case of H implantations, certain experiments were made with samples implanted through and subsequently annealed with a thin SiO₂ capping layer. The role of SiO₂ is to artificially maintain hydrogen in the sample up to higher annealing temperatures.^{9,17,18}

II. EXPERIMENTAL PROCEDURE

In this study, Philips 25% ⁵⁷Fe enriched YIG single crystals have been used. (These fine samples were made by our late colleague J. M. Robertson from Philips Research Laboratory, Eindhoven.) They were grown by liquid epitaxy on a (111)-oriented Gd₃Ga₅O₁₂ substrate. The large enrichment in ⁵⁷Fe allowed us to obtain a very good accuracy in Mössbauer spectra.

Hydrogen implantations were performed using a low beam current in order to limit thermal effects and with samples tilted 7° off the <111> axis to avoid channeling effects. Samples were sequentially implanted with 4 × 10¹⁶ H₂⁺/cm² at an energy of 80 keV, 2 × 10¹⁶ H₂⁺/cm² at 50 keV, and 1 × 10¹⁶ H₂⁺/cm² at 20 keV. From previous hydrogen profile determinations¹⁸ it can be deduced that in our samples the whole implanted hydrogen is located inside a depth of 400 nm. We used two higher doses in order to have a reservoir of hydrogen for subsequent annealing treatments, whereas the hydrogen implanted at 20 keV is located within the first 100 nm corresponding to the analyzed thickness by CEMS. Moreover, two kinds of samples were used, one with a 10-nm-thick SiO₂ capping layer deposited before implantation by sputtering technique and the other without this layer. Far from being as effective as thicker layers in preventing hydrogen effusion,¹⁸ the choice of such a thin SiO₂ layer was made so as to obtain identical implantation effects as with uncovered films before annealings.

The neon implantation was carried out at an energy of 50 keV and a dose of 7 × 10¹³ Ne⁺/cm². Such a low dose allows us to assert no amorphization of the crystal.⁷ Under these conditions the Ne⁺ distribution is located within a 100-nm-thick layer and also the whole density of defects is made comparable to the same analyzed region as the H₂⁺ implanted samples. This does not imply identical microscopic defect structures.

Mössbauer-spectroscopy measurements were achieved at room temperature (RT) and liquid nitrogen temperature (LNT) using the CEMS technique. This very sensitive technique applied to ⁵⁷Fe enriched samples permits very-well-defined spectra to be obtained. This point is particularly important, taking into account the complexity of Mössbauer garnet spectra. Two experimental setups have been used. The spectra obtained with unimplanted and

Ne-implanted samples were measured with a helium flow proportional counter in which samples were placed in backscattering geometry (i.e., the γ -ray incidence angle was 90°). This geometry is convenient in determining the orientation of hyperfine magnetic fields.

In the case of H-implanted garnets the conversion electrons were selected and focused by means of magnetic coils on channeltron detectors. This Mössbauer device, described by Massenot,¹⁹ allows a rather good selection of the conversion electrons coming from the implanted layer only. A 70-mCi ⁵⁷CoRh source delivered a γ -ray beam which made a 30° angle with the surface of the sample. This angle must be taken into consideration for the determination of the magnetization direction. In fact, when this direction is not perpendicular to the surface, its determination is rather difficult because of lack of symmetry around the incident γ -ray beam. Later on, only changes in the direction of the magnetization will be discussed.

The conversion-electron Mössbauer spectra were measured using a constant acceleration triangular drive. After a folding to provide a constant background, CEMS spectra were fitted using a least-squares minimization routine on the Institut National de Physique Nucléaire et de Physique des Particules (IN2P3) Control Data Corporation Cyber-750 computer with the assumption of Lorentzian shapes of Mössbauer lines. The velocity scale and all the data are referred to a metallic iron absorber at room temperature.

Isochronal thermal treatments in air were performed from 200 to 900°C for 30 min at each temperature. After each annealing step the samples were quenched to room temperature. Infrared absorption spectra of the implanted samples were obtained with a 3600 Nicolet Fourier transform spectrometer.

III. CHARACTERIZATION OF VIRGIN YIG SAMPLES

The crystallographic structure of YIG has been reviewed by Winkler²⁰ and the combined hyperfine interactions in YIG have been studied recently by Winkler *et al.*²¹ using Mössbauer spectroscopy. YIG belongs to the space group O_h^{10} ($Ia\bar{3}d$); the 24 iron *d* sites are divided into three different groups of eight iron atoms each with a different symmetry axis ([100], [010], and [001]) and the 16 *a* sites are divided into four different groups of four iron atoms each with directions of the electric field gradient V_{zz} in [111], [$\bar{1}\bar{1}\bar{1}$], [$\bar{1}\bar{1}1$], and [$\bar{1}1\bar{1}$] directions. Thus, in the most general case, up to seven combined hyperfine interactions can appear with different angles between the various V_{zz} and the direction of magnetization. In the study of Winkler *et al.*,²¹ depending on the choice of the direction of an external bias field, the number of Mössbauer spectra varies between 3 and 4. For polycrystalline garnets the corresponding number of Mössbauer spectra is reduced to one *d* site and two *a* sites. Generally, most of the papers concerned with the determination of hyperfine fields in YIG assume the existence of these three contributions only. In the present experiments the samples are not polarized but the spectral resolution allows us to consider four subspectra: two *a* sites and two

d sites with different hyperfine parameters [isomer shift (IS), quadrupole splitting (QS), hyperfine field (HF), direction of the magnetization]. In Fig. 1 the spectra obtained with a virgin YIG by means of the He proportional counter or channeltron setup, respectively, are displayed. The fits of these spectra are really improved when four instead of three subspectra are considered. The values obtained from computer fits are summarized in Table I. W , $A_{2,5}/A_{1,6}$, and RI are the linewidths, areal ratios of the second or fifth to the first or sixth lines, and relative intensities of each component, respectively. Δ is the experimental difference [(6-5)-(1-2)] of the line positions in the hyperfine patterns and is roughly proportional to the product $\frac{1}{2}eQV_{zz}(3\cos^2\theta-1)$ in which θ is the angle between the hyperfine magnetic field and the electric field gradient. The hyperfine parameters are in very good agreement with the published data (Ref. 21 and references therein). The ratio 1.56(14) of tetrahedral to octahedral sites verifies the 1.5 theoretical predicted value. The values obtained for a measurement performed at liquid nitrogen temperature with the channel electron detector setup are also reported. The ratios of hyperfine fields measured at LNT and RT are 1.17(1) and 1.13(1) for d sites and a sites, respectively. They confirm that the hyperfine

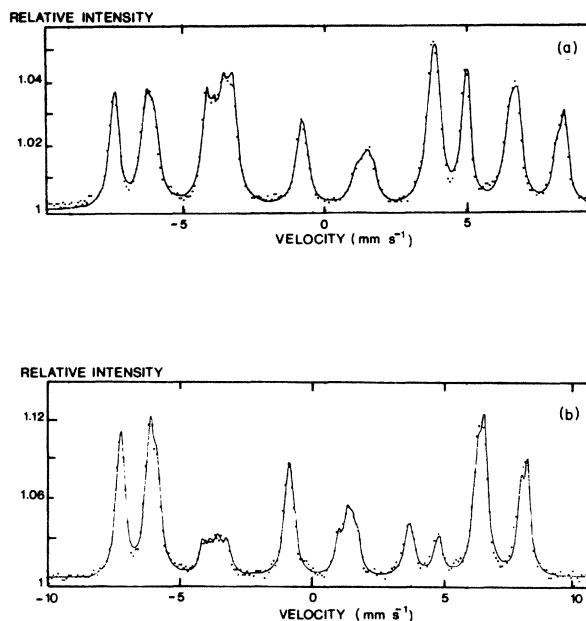


FIG. 1. CEMS spectra obtained with (a) the proportional counter and (b) the channeltron setup for a virgin YIG single crystal.

TABLE I. Virgin YIG single crystal. Mössbauer parameters obtained by computer fitting of the spectra measured with the proportional counter and with the channeltron setup at room temperature (RT) and liquid nitrogen temperature (LNT). IS, isomer shift (referred to α iron); HF, hyperfine field; Δ , quadrupole splitting; $A_{2,5}/A_{1,6}$, ratio of the second or fifth to the first or sixth lines; W , linewidth; RI, relative intensity (IS, Δ , and W in mm s^{-1} , HF in kOe).

		Gas-flow counter	Channeltron setup	
		RT	RT	LNT
a site	IS	0.39(1)	0.38(2)	0.52(3)
	HF	493(2)	493(2)	551(1)
	Δ	0.14(4)	0.10(6)	0.09(3)
	$A_{2,5}/A_{1,6}$	1.08(5)	0.23(2)	0.58(5)
	W	0.33(3)	0.30(2)	0.42(2)
	RI	0.23(1)	0.23(2)	0.22(2)
a' site	IS	0.39(2)	0.38(3)	0.43(3)
	HF	481(2)	480(3)	545(2)
	Δ	-0.16(5)	-0.11(5)	-0.11(6)
	$A_{2,5}/A_{1,6}$	1.1(1)	0.25(5)	0.43(5)
	W	0.33(3)	0.30(2)	0.42(2)
	RI	0.15(1)	0.16(2)	0.18(2)
d site	IS	0.14(2)	0.13(2)	0.23(3)
	HF	407(2)	404(4)	475(1)
	Δ	0.09(3)	0.09(5)	0.08(8)
	$A_{2,5}/A_{1,6}$	1.1(1)	0.29(3)	0.57(6)
	W	0.40(2)	0.39(3)	0.47(2)
	RI	0.30(3)	0.37(2)	0.40(4)
d' site	IS	0.19(2)	0.18(1)	0.32(1)
	HF	391(2)	387(3)	461(1)
	Δ	-0.05(3)	-0.09(3)	-0.22(4)
	$A_{2,5}/A_{1,6}$	1.2(1)	0.29(3)	0.65(10)
	W	0.42(3)	0.38(3)	0.47(5)
	RI	0.30(3)	0.24(2)	0.21(4)

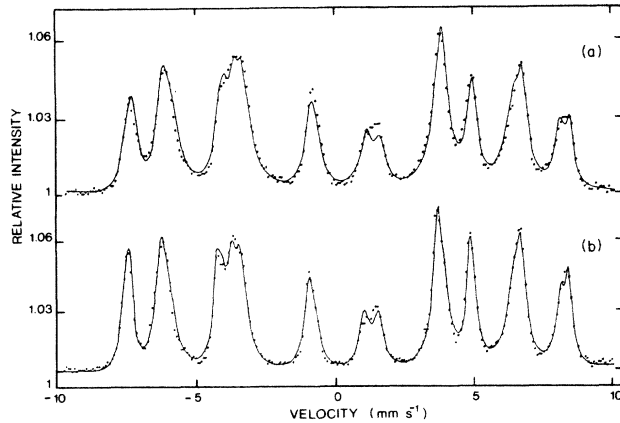


FIG. 2. CEMS spectra obtained with the proportional counter for (a) a neon as-implanted YIG single crystal and (b) after annealing in air at 850°C.

fields follow the variation in magnetization as calculated by Pauthenet.²² These ratios agree with those obtained by Bauminger *et al.* (1.16 and 1.11) by Mössbauer spectroscopy²³ and Ogawa *et al.* (1.20 and 1.13) by NMR measurements.²⁴

From the $A_{2,5}/A_{1,6}$ ratios in the spectrum of Fig. 1(a)

the magnetization direction relative to the surface normal makes an angle of $71 \pm 5^\circ$. This spin tilt angle is exactly the same as found by Balestrino²⁵ on a similar sample. The changes in the ratio $A_{2,5}/A_{1,6}$ measured with the channeltron setup is due to the different incident angle of the γ -ray beam as explained in Sec. II.

IV. NEON-IMPLANTED YIG

In Fig. 2 are displayed the CEMS spectra obtained with the proportional counter setup for a neon as-implanted YIG single crystal and after annealing in air up to 850°C. The fitted parameters obtained for a similar sample before and after neon implantation as well as annealed at 850°C are collected in Table II.

After implantation, the hyperfine fields are slightly reduced, whereas the linewidths are broadened. These two effects result from the implantation damage as observed previously in the case of bubble garnets and pure YIG.¹⁰⁻¹³ One has to mention that the linewidths are wider for tetrahedral sites than for octahedral sites, this effect being more pronounced for the d' sites. Moreover, a paramagnetic component is not observed in agreement with other studies.¹¹⁻¹³ In fact, for such a low dose there is no amorphization of the garnet. The magnetization

TABLE II. Fitted parameters of Mössbauer spectra, measured with the proportional counter, corresponding to a virgin YIG single crystal before implantation, after implantation with neon, and subsequently annealed in air at 850°C.

		Virgin YIG	Neon-implanted YIG	
			As-implanted	Annealed at 850°C
a site	IS	0.39(1)	0.40(1)	0.40(1)
	HF	497(1)	486(1)	491(1)
	Δ	0.3(1)	0.43(3)	0.36(3)
	$A_{2,5}/A_{1,6}$	1.12(16)	0.88(3)	0.95(5)
	W	0.29(3)	0.36(2)	0.30(2)
	RI	0.18(4)	0.17(1)	0.20(2)
a' site	IS	0.38(1)	0.34(1)	0.37(1)
	HF	489(3)	482(1)	487(1)
	Δ	-0.18(6)	-0.49(2)	-0.42(2)
	$A_{2,5}/A_{1,6}$	0.85(8)	0.90(2)	0.85(3)
	W	0.34(1)	0.37(1)	0.36(1)
	RI	0.20(4)	0.17(1)	0.18(1)
d site	IS	0.16(1)	0.12(1)	0.11(2)
	HF	401(2)	404(1)	405(2)
	Δ	0.64(3)	0.26(2)	0.32(5)
	$A_{2,5}/A_{1,6}$	1.24(9)	0.73(5)	0.70(7)
	W	0.34(2)	0.39(3)	0.37(5)
	RI	0.22(2)	0.23(3)	0.25(2)
d' site	IS	0.18(1)	0.18(1)	0.19(1)
	HF	400(2)	385(1)	389(3)
	Δ	-0.37(2)	-0.04(2)	-0.05(4)
	$A_{2,5}/A_{1,6}$	1.00(5)	1.33(-5)	1.33(-5)
	W	0.48(2)	0.73(4)	0.60(3)
	RI	0.40(1)	0.43(3)	0.37(2)

directions of the octahedral sites are not affected by the neon implantation, whereas the magnetization directions of the tetrahedral sites are markedly changed. Moreover, it can be also seen that the changes for d and d' sites are not correlated. This effect is not annealed up to 850°C.

After annealings only small evolutions are observed up to 850°C, mostly a slight increase for the HF values. This can be compared to the observation of Picone and Morrish who found that some damage remains after anneals up to 700°C (Ref. 13) in a bubble garnet and that of Awano *et al.*²⁶ who have shown recently by x-ray rocking curve measurements that strain in a neon-implanted (Ga,Tm,Ga):YIG goes to zero at an annealing temperature of 1100°C only. However, they have also shown that a

700°C annealing is sufficient to restore completely the magnetization.

V. HYDROGEN-IMPLANTED YIG

The H_2^+ triple implantation was performed in pure or SiO_2 capped YIG single crystals. We first present the results obtained with uncovered samples.

Thermal treatments were performed at 200, 350, 450, 650, and 850°C. In Table III the fitted parameters are compiled and in Fig. 3 are presented the CEMS spectra obtained for as-implanted and 200, 450, and 850°C annealed samples. Just after hydrogen implantation the hyperfine fields are systematically lowered and their distri-

TABLE III. Mössbauer hyperfine parameters of fitted spectra corresponding to a H_2^+ as-implanted YIG single crystal and isochronally annealed for 30 min at temperatures of 200, 350, 450, 650, and 850°C.

		As-implanted	200°C	350°C	450°C	650°C	850°C
a site	IS	0.34(1)	0.37(2)	0.38(2)	0.38(2)	0.38(1)	0.38(3)
	HF	468(1)	474(1)	475(1)	475(3)	477(1)	482(1)
	Δ	0.12(2)	0.03(4)	0.06(3)	0.04(4)	0.07(4)	0.08(4)
	$A_{2,5}/A_{1,6}$	0.20(3)	0.23(5)	0.22(3)	0.28(3)	0.20(3)	0.18(3)
	W	0.52(3)	0.52(5)	0.51(4)	0.50(3)	0.48(3)	0.46(2)
	RI	0.23(3)	0.27(5)	0.28(3)	0.27(3)	0.26(2)	0.26(2)
a' site	IS	0.40(2)	0.36(3)	0.30(3)	0.32(3)	0.30(1)	0.28(2)
	HF	447(4)	457(3)	462(3)	463(3)	462(2)	470(2)
	Δ	0	0	0	0	0	0
	$A_{2,5}/A_{1,6}$	0.40(5)	0.40(5)	0.35(5)	0.35(5)	0.35(5)	0.35(5)
	W	0.50(4)	0.43(8)	0.35(5)	0.41(5)	0.36(3)	0.33(3)
	RI	0.08(2)	0.08(3)	0.07(2)	0.08(2)	0.07(1)	0.08(2)
d site	IS	0.11(2)	0.17(2)	0.18(2)	0.15(2)	0.14(1)	0.13(2)
	HF	386(1)	390(1)	391(3)	392(4)	394(1)	396(2)
	Δ	0.18(3)	0.12(5)	0.15(6)	0.11(5)	0.10(4)	0.16(5)
	$A_{2,5}/A_{1,6}$	0.18(5)	0.28(10)	0.23(4)	0.20(5)	0.19(5)	0.22(5)
	W	0.70(5)	0.60(5)	0.52(4)	0.55(5)	0.51(3)	0.43(3)
	RI	0.36(4)	0.33(5)	0.30(2)	0.28(4)	0.28(2)	0.29(2)
d' site	IS	0.20(2)	0.16(4)	0.12(4)	0.16(2)	0.19(1)	0.22(4)
	HF	361(1)	375(2)	380(5)	379(5)	380(5)	384(3)
	Δ	-0.04(4)	-0.15(5)	-0.06(3)	-0.10(2)	-0.14(2)	-0.17(10)
	$A_{2,5}/A_{1,6}$	0.60(10)	0.50(10)	0.43(8)	0.43(5)	0.35(5)	0.22(5)
	W	0.92(5)	0.85(5)	0.80(10)	0.57(5)	0.69(5)	0.65(5)
	RI	0.22(3)	0.23(3)	0.23(3)	0.22(3)	0.22(3)	0.22(3)
d_H site	IS	0.18(3)	0.18(2)	0.19(2)	0.18(3)	0.15(3)	0.18(3)
	HF	337(2)	342(1)	346(1)	346(5)	346(7)	349(6)
	Δ	0	0	0	0	0	0
	$A_{2,5}/A_{1,6}$	0.40(5)	0.40(5)	0.35(5)	0.35(5)	0.35(5)	0.35(5)
	W	0.65(10)	0.65(10)	0.63(4)	0.60(3)	0.66(9)	0.65(5)
	RI	0.08(3)	0.07(2)	0.09(2)	0.11(2)	0.12(3)	0.11(2)
D	IS	0.33(3)	0.30(2)	0.30(2)	0.28(5)	0.27(3)	0.28(3)
	Δ	2.5(1)	2.40(3)	2.47(4)	2.37(3)	2.30(5)	2.37(5)
	W	0.30(5)	0.29(2)	0.29(2)	0.30(3)	0.32(3)	0.27(3)
	RI	0.03(2)	0.02(1)	0.03(1)	0.04(2)	0.05(2)	0.04(2)

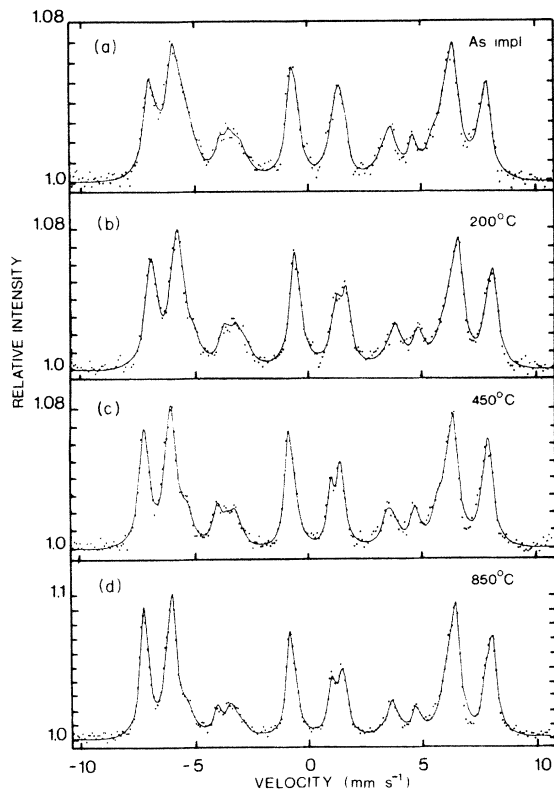


FIG. 3. CEMS spectra of H_2^+ -implanted crystal obtained with the channeltron setup for as-implanted sample and for 200, 450, and 850°C annealed samples.

butions are more broadened than after neon implantation. From Fig. 3 it is obvious that the overall magnetization direction is not much changed. The d' component seems the most affected: There is a (i) very large broadening of the linewidths with an asymmetric hyperfine-fields distribution as observed in the case of neon implantation and (ii) larger change in the direction of the hyperfine field. The fitting of the spectra is improved by considering a weak quadrupole doublet (D) of about 3% for the intensity and having a large QS (2.5 mm s^{-1}) as indicated in Fig. 3. This means that the superexchange interactions are destroyed in a small part of the implanted layer only.

The salient point is the creation of a new magnetic component (d_H) with a hyperfine field of 337 kOe and 0.18 mm s^{-1} for the isomer shift. The existence of such a component has been suggested by Morrish *et al.* in the case of a bubble garnet film implanted with H_2^+ ions, but no explanation concerning its origin was proposed.¹⁴ This new component d_H is unambiguously due to a modification of part of the tetrahedral sites on account of both the value of the isomer shift and the sum of the contributions of d , d' , and d_H sites, which corresponds roughly to the total of d and d' sites in the virgin sample. As this component does not exist after a neon implantation, its origin has to be attributed to either qualitatively different damage caused by hydrogen implantation¹⁶ or chemical effect due to the presence of hydrogen in the lattice.^{6,8}

To verify this last hypothesis, infrared absorption measurements were performed at room temperature. Bubble garnet single crystals $(Y,Sm,Lu,Ca)_3(Fe,Ge)_5O_{12}$ were sequentially implanted with 10^{17} cm^{-2} protons or deuterons at 80 keV and 10^{17} cm^{-2} at 150 keV. The ir spectra obtained directly after implantations are presented in Figs. 4(a) and 4(b) for proton- and deuterium-implanted samples, respectively. The absorption bands located near 3590 cm^{-1} in the hydrogen-implanted sample and 2630 cm^{-1} in the deuterium-implanted sample are characteristic of the presence of O—H and O—D chemical bonds. From the surface of these absorption bands, using the method described by Gruen *et al.*²⁷ and after correction for the refractive index of the medium, the number of O—H or O—D bonds formed in the implanted zone can be estimated: about $3 \cdot 10^{16} \text{ cm}^{-2}$ O—H or O—D. This value compared with the implanted ion doses ($2 \cdot 10^{17} \text{ cm}^{-2}$) indicates that only a small part of the implanted ions ($\approx 15\%$) are stabilized in the matrix in the form of simple hydroxyl or deuteroxyl radicals. However, we must note that the local concentration of O—H bonds formed in the implanted zone represents about 11% of the total number of iron ions in tetrahedral sites. This value is comparable to the relative intensity of the Mössbauer component d_H observed in the hydrogen-implanted YIG [see Table III, as-implanted crystal: $I(d_H)/I(d+d'+d_H)=12\%$]. Final-

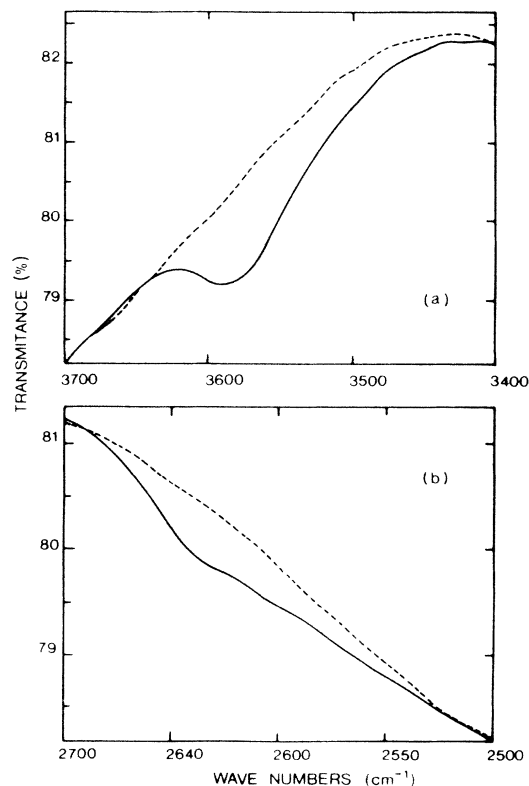


FIG. 4. ir spectra of garnet crystals implanted with (a) protons and (b) deuterons.

ly, it seems that the formation of O—H bonds which perturbs preferentially the iron ions in tetrahedral sites is responsible for the d_H component characteristic of hydrogen implantation in YIG.

Annealing at 200°C produces an increase of the hyperfine fields. This enhancement continues for the annealing at 350°C with a narrowing of the lines. The CEMS spectra do not evolve between 350 and 650°C. Annealing at 850°C again increases the hyperfine fields. These three annealing stages have been determined by Suran *et al.*⁶ by measuring the lattice constant strain $\Delta a_1/a$ and were interpreted by assuming that the contribution to the lattice strain arises from two different mechanisms: displacement of the lattice ions due to the implantation and presence of hydrogen in the implanted layer. The evolution observed for annealings up to 350°C can be explained by the large desorption rate of hydrogen which occurs in this temperature range, whereas above 650°C a restoration of the lattice damage takes place. This is correlated with the ir absorption measurements: The O—H and O—D bands detected just after implantation remain after an annealing at 200°C and disappear when the annealing temperature is 450°C. It is surprising that the d_H component persists even after an anneal at 850°C when hydrogen has completely diffused out of the garnet. Its evolution follows that of the other components which are connected with the lattice damage restoration.

To avoid the important loss of hydrogen in the garnet for the low annealing temperatures, the same study was carried out with a SiO₂ capped garnet. Annealing temperatures were 200, 250, 300, and 450°C with the SiO₂ layer. After this last annealing the SiO₂ layer was removed. Again an annealing at 450°C was performed and followed by annealings at 650 and 900°C. In Fig. 5 the CEMS spectra corresponding to the as-implanted sample and the 200, 450, and 900°C annealed samples are presented. The same phenomena observed with the uncovered samples are present: a decrease of the hyperfine fields, large linewidths, no rocking of the magnetization, and a weak quadrupole doublet and d_H component. The only differences could be a slightly more important contribution of the d_H component [RI is equal to 13(1)%] with a rather small isomer shift [IS is equal to 0.09(2) mm s⁻¹] and a stronger decrease in the fields of the octahedral sites [HF(*a*) is equal to 457(1) kOe, HF(*a'*) is equal to 426(2) kOe].

After the first anneal at 200°C the hyperfine field's increase is less than that for the uncovered garnet; even the HF values of d' and d_H components diminish. As the implanted hydrogen cannot escape very easily, an explanation could be an increase in the H interaction perturbing tetrahedral sites or a pressure action due to the presence of hydrogen.⁹ The behavior upon thermal treatments up to 450°C is the same as previously with only a shift towards lower HF values.

When the SiO₂ layer is removed and after a subsequent anneal at 450°C, no significant difference is observed except a decrease of the HF values. In fact, with only the 10-nm-thick SiO₂ layer, after annealing at 450°C all the hydrogen has diffused out of the sample and this decrease can be explained by a hold of the surface strain induced

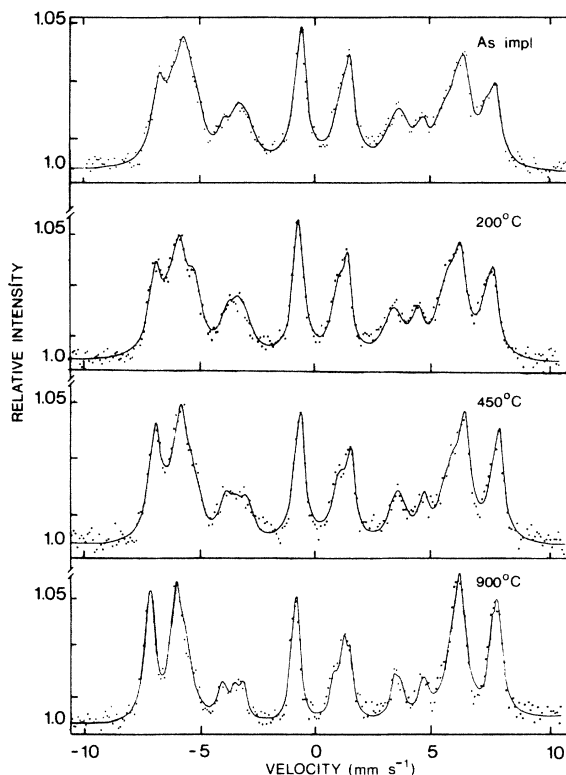


FIG. 5. CEMS spectra corresponding to SiO₂ capped garnet implanted with H₂⁺ and annealed at 200, 450, and 900°C.

by the SiO₂ layer.⁹ As in the previous study there is no appreciable change between 450 and 650°C, and after annealing at 900°C the lattice begins to be restored (increase of HF, narrowing of lines) but always with a persistence of the d_H component.

VI. DISCUSSION

The CEMS technique applied to ⁵⁷Fe enriched YIG has allowed us to obtain good resolutions of the spectra. Its association with the ir spectroscopy technique has permitted us to show clearly the specific chemical effect of hydrogen implantation in comparison with a pure damage effect from a shallow neon implantation.

Just after the neon implantation it is obvious that the half-widths of the *d*-site lines are broader than the half-widths of the *a*-site lines. This can be related to the fact that the *d* sites exhibit a strong magnetic interaction with *a* and *c* sites²⁸ giving rise to a large distribution of HF coming from the perturbation in the three sublattices. The line broadening is even more important in the case of H₂⁺ implantations. As doses and energies of Ne and H implantations have been chosen to create macroscopically similar amounts of defects, the difference in line broadness has to be correlated either to different sorts of defects or to some specific chemical interaction. According to the first hypothesis, Matsutera *et al.*¹⁶ have shown that H as compared to Ne produces nuclear collisions with an en-

ergy transfer ten times smaller. This leads to an inhomogeneously damaged implanted zone with individual dense cascades for Ne, whereas H implantation produces a more homogeneous dispersion of point defects in the implanted volume. So the structure and density of aggregated defects must be different in the two considered systems. However, the second hypothesis, already proposed by Morrish *et al.*¹⁴ for H-implanted bubble garnet material, is supported by the creation of a new magnetic site, d_H , among the tetrahedral sites after the hydrogen implantation. This component can be correlated with the formation of O—H bonds detected by ir absorption measurements and would be only concerned with a small fraction of the total implanted hydrogen ($\sim 15\%$); the remaining part would be responsible for some internal pressure creation and/or for the reduction of iron giving rise to the observed line broadening. A surprising effect has to be underlined—it is the existence of the d_H component up to a 850°C annealing. This could come from some strain built up during the O—H bond formation which remains after the O—H hydrolysis between 200 and 350°C. The hypothesis of the correlation between O—H and d_H is also supported by the recent works of Hisatake.¹⁵ He has performed CEMS measurements as a function of depth and has observed the presence of the d_H component only in the spectra corresponding to the hydrogen stopping region. As a matter of fact, the persistence of broad lines of the d and d' sextets above 450°C when the hydrogen is completely diffused out of the garnet⁹ is also remarkable. It seems that the reduction effect as well as the O—H bond formation affect preferentially iron in tetrahedral environments. It is also worth remembering that this 450°C annealing temperature corresponds to the complete oxidation of iron in Fe-implanted garnets.²⁹ A reduction mechanism has been proposed by Pascard³⁰ who considers the transformation of ion pairs $[O^{2-}-Fe_d^{3+}]$ into $[O^- - Fe_d^{2+}]$ resulting from an electron jump from O_2^- anions to the nearest-neighboring Fe^{3+} cations in

tetrahedral sites. Here H^+ ions would act as a charge compensator in the vicinity of the ferrous complex. Also, Milani and Paroli³¹ have shown the formation of hydroxyl radicals and the presence of Fe^{2+} in tetrahedral sites in hydrogen-diffused YIG. Anyway, whether from a ferrous complex or through O—H bond formation, only the tetrahedral sites seem to be concerned with the specific chemical effect of hydrogen.

A last and interesting observation has to do with the sole progressive changes in the direction of the magnetization of d' sites ($A_{2,5}/A_{1,6}$) in the course of the different annealings up to 850°C (see Table III), the magnetization directions of the other sites remaining unchanged.

For neon-implanted crystals, similar tiltings of the magnetization directions are observed having an effect upon both d and d' sites. This difference in the d orientation, which is not affected in the case of H implantation, could be related to the different damage structures previously discussed. Yet in this case there is no annealing effect on the magnetization tilt up to 850°C. This tilt angle variation between Fe sites could be part of the origin of the peculiar Faraday rotation θ_F behavior obtained in annealed implanted garnets.³²

Some further studies with complementary techniques well adapted to the study of iron reduction by hydrogen would be very useful.

ACKNOWLEDGMENTS

We are indebted to Professor E. Gerdau (University of Hamburg), Professor H. Winkler (University of Lubeck), and Dr. G. Balestrino (Consiglio Nazionale delle Ricerche, Roma) for fruitful comments and discussions for the interpretation of Mössbauer components in virgin YIG. We also thank Dr. P. F. Bongers and Dr. U. Enz from Philips Research Laboratory, Eindhoven for permitting us to use their enriched samples.

¹A. H. Eschenfelder, *Magnetic Bubble Technology* (Springer, Berlin, 1980).

²P. Hansen and J. P. Krumme, *Thin Solid Films* **114**, 69 (1984).

³P. Paroli, *Thin Solid Films* **114**, 187 (1984).

⁴P. Gerard, *Thin Solid Films* **114**, 1 (1984).

⁵R. Hirko and K. Ju, *IEEE Trans. Magn.* **MAG-16**, 958 (1980).

⁶G. Suran, H. Jouve, and P. Gerard, *J. Appl. Phys.* **54**, 2006 (1983).

⁷V. S. Speriosu and C. H. Wilts, *J. Appl. Phys.* **54**, 3325 (1983).

⁸H. Makino, Y. Hidaka, and H. Matsutera, *J. Magn. Magn. Mater.* **35**, 311 (1983).

⁹P. Gerard, P. Martin, and M. T. Delaye, *J. Appl. Phys.* **57**, 4058 (1985).

¹⁰G. P. Skrimshire, G. Longworth, and G. Dearnaley, *J. Phys. D* **12**, 1951 (1979).

¹¹P. J. Picone and A. H. Morrish, *Solid State Commun.* **34**, 743 (1980).

¹²P. H. Smit, H. A. Algra, and J. M. Robertson, *J. Appl. Phys.* **52**, 2364 (1981).

¹³P. J. Picone and A. H. Morrish, *J. Appl. Phys.* **53**, 2471 (1982).

¹⁴A. H. Morrish, P. J. Picone, and N. Saegusa, *J. Magn. Magn. Mater.* **31–34**, 923 (1983).

¹⁵K. Hisatake (private communication).

¹⁶H. Matsutera, S. Esho, and Y. Hidaka, *J. Appl. Phys.* **53**, 2504 (1982).

¹⁷Y. Sugita, T. Takeuchi, and N. Ohta, in *Proceedings of the Conference on Magnetism and Magnetic Materials*, Atlanta, 1981 (unpublished).

¹⁸J. Magnin, P. Gerard, H. Jouve, and J. P. Thomas, *Nucl. Instrum. Methods* **209/210**, 1153 (1983).

¹⁹O. Massenot, *Nucl. Instrum. Methods* **153**, 419 (1978).

²⁰G. Winkler, *Magnetic Garnets*, Vol. 5 of *Vieweg Tracts in Pure and Applied Physics* (Vieweg, Braunschweig, 1981).

²¹H. Winkler, R. Eisberg, E. Alp, R. Ruffer, E. Gerdau, S. Lauer, A. X. Trautwein, M. Grodzicki, and A. Vera, *Z. Phys.* **B 49**, 331 (1983).

²²R. Pauthenet, *Ann. Phys. (Paris)* **3**, 424 (1958).

²³R. Bauminger, S. G. Cohen, A. Marinov, and S. Ofer, *Phys. Rev.* **122**, 743 (1961).

²⁴S. Ogawa and S. Morimoto, *J. Phys. Soc. Jpn.* **17**, 654 (1962).

²⁵G. Balestrino (private communication).

- ²⁶H. Awano, V. S. Speriosu, and C. H. Wilts, *J. Appl. Phys.* **55**, 3043 (1984).
- ²⁷D. M. Gruen, B. Siskind, and R. B. Wright, *J. Chem. Phys.* **65**, 363 (1976).
- ²⁸L. Néel, R. Pauthenet, and B. Dreyfus, *Prog. Low Temp. Phys.* **4**, 344 (1964).
- ²⁹A. Pérez, G. Marest, P. Gérard, M. Madore, and P. Martin, *Nucl. Instrum. Methods* **209/210**, 1179 (1983).
- ³⁰H. Pascard, *Phys. Rev. B* **30**, 2299 (1984).
- ³¹E. Milani and P. Paroli, *J. Appl. Phys.* **55**, 2173 (1984).
- ³²P. Hansen, H. Heitmann, and H. A. Algra, *IEEE Trans. Magn.* **MAG-19**, 1769 (1980).